Secondary-electron production cross section for 800-eV electron-impact ionization of carbon monoxide

Ce Ma and R. A. Bonham
Department of Chemistry, Indiana University, Bloomington, Indiana 47405
(Received 8 January 1988)

Measurements of the doubly differential cross sections with respect to the ejected energy W and the solid angle of detection for electron-impact ionization of carbon monoxide are reported at an incident energy of 800 eV. The ejected angle was varied from 30° to 150° in steps of 15°. The cross sections were obtained by use of a crossed-beam time-of-flight apparatus with an effusive gas source and pulsed electron beam. The relative measurements were placed on an absolute scale by matching the experimental elastic differential cross sections to absolute measurement. Singly differential and total ionization cross sections are presented along with an analysis of the near-threshold autoionization spectrum.

The electron-impact cross-section differential with respect to the solid angle of ejection and ejected energy of secondary electrons produced by collisions with atoms and molecules is becoming an increasingly important quantity for simulation studies of radiation damage and plasma behaviors. This Brief Report presents new data to supplement existing data obtained at lower incident energy.[1] The details of the apparatus have been published elsewhere.[2] In summary, the apparatus consisted of a pulsed electron source obtained by sweeping an electron beam produced from a commercially available electron gun across a skimmer with an aperture 1 mm in diameter. The electron pulse intersects at a right angle an effusive gas beam produced by expanding gas out of a hypodermic needle into the vacuum chamber. The scattering angle was variable from 30° to 150°. The unscattered beam was monitored by use of a detector in the forward direction.

The energy analysis of the electron spectrum is obtained using standard time-of-flight (TOF) techniques.[2] The scattered and secondary electrons are allowed to drift for 432 mm in the field-free region between the scattering center and a graphite-coated copper grid located 6 mm in front of the surface of the electron detector, which consisted of two microchannel plates (MCP's) arranged in a chevron configuration. The magnetic field around the apparatus was reduced to less than 2 mG by use of a Helmholtz coil pair and μ-metal shields. The electronics used in this experiment was the same as that used in Ref. 2.

The conversion from the background-subtracted TOF intensity I_{sc} to the doubly differential cross section (DDCS) $d^2\sigma(W,\theta)/dW\,d\Omega$ was carried out by use of the relation

$$\frac{d^2\sigma(W,\theta)}{dW d\Omega}=c\frac{I_{sc}}{\eta(W)\varepsilon(W)(dW/dt)}\ , \tag{1}$$

where c is a normalization constant obtained by matching the experimental elastic differential cross sections (EDCS's) to the absolute EDCS measurement of DuBois and Rudd;[3] dW/dt is the time-to-energy conversion function, and $\varepsilon(W)$ is the fractional attenuation of the scattered electron current of energy W by the residual gas. In order to calculate $\varepsilon(W)$, we used the total cross-section data of Kwan *et al.*;[4] $\eta(W)$ is the relative detector efficiency.[5]

Opal, Beaty, and Peterson[1] published e-CO DDCS data with 500-eV incident electron energy and ejected electron energies from 4.13 to 205 eV over the ejected angle range from 30° to 150°. Our 800-eV incident electron energy data were obtained in the ejected electron energy region from 0.93 to 393 eV and over the same angular region. In general, the two data sets have similar shapes but the DDCS for the 800 eV is 6% to 40% smaller.

For low-ejected energies it has been shown[2] that an expansion of the type

$$\frac{d^2\sigma(W,\theta)}{dW d\Omega}=\sum_{n=0}^{N}A_n(W)P_n(\cos\theta) \tag{2}$$

provides a convenient and accurate means for representing ejected electron angular distributions where P_n is the nth-order Legendre polynomial and the coefficient $A_n(W)$ is a function of the ejected energy W and the incident electron energy T. Coefficients $A_n(W)$ are given in Table I.

The DDCS integrated over the ejected angle generated the singly differential cross section (SDCS)

$$\frac{d\sigma(W)}{dW}=4\pi A_0(W)\ . \tag{3}$$

The error in the SDCS was estimated to be 3% for A_0 determined by use of Eq. (2) with $N=4$. The uncertainty was determined from the variation in A_0 for fits with $N=3-5$. In addition, counting errors and other systematic errors lead to a total estimated uncertainty of $\pm 15\%$ in the SDCS. Most of the error comes from uncertainties in the normalization process.

The SDCS can best be viewed by use of a Platzmann plot that is a modified SDCS denoted as $Y(E,T)$ and plotted as a function of R/E where[6]

TABLE I. Coefficients $A_n(W)$.

W (eV)	A_0	A_1	A_2	A_3	A_4
0.93	61.78	−4.04	−22.64	−5.17	−17.63
1.01	60.57	−3.70	−26.35	−2.10	−17.32
2.04	53.82	−6.00	−8.16	−1.15	−1.36
3.00	44.64	−1.91	−5.97	−2.91	−0.44
4.02	38.19	−1.51	−7.95	−2.88	−0.73
5.01	36.71	−1.42	−8.28	−1.47	2.08
6.08	32.37	−0.58	−5.59	−1.79	2.74
7.02	29.44	−0.62	−5.10	−0.58	1.94
8.10	27.92	−0.40	−6.05	−2.27	1.56
9.08	28.12	0.54	−6.05	−2.09	2.69
10.1	26.15	0.14	−5.90	−2.59	1.77
12.0	22.18	0.43	−5.29	−2.42	1.76
14.0	18.80	0.99	−4.99	−2.40	1.26
16.1	15.78	1.01	−4.26	−2.17	1.38
18.2	13.15	1.29	−4.12	−2.03	1.29
20.0	11.45	1.10	−3.70	−2.30	0.91
25.1	8.45	1.26	−3.05	−1.91	0.68
30.1	6.53	1.15	−2.71	−1.97	0.92
35.8	4.98	1.05	−2.29	−1.83	0.59
40.9	3.88	0.82	−1.82	−1.69	0.36
45.9	3.14	0.71	−1.43	−1.50	0.28
50.2	2.67	0.66	−1.29	−1.39	0.17
60.9	1.81	0.54	−0.88	−1.13	0.08
70.0	1.35	0.44	−0.72	−1.03	0.01
91.8	0.77	0.34	−0.42	−0.74	−0.14
104	0.58	0.29	−0.30	−0.60	−0.16
126	0.39	0.26	−0.18	−0.44	−0.20
146	0.29	0.22	−0.11	−0.34	−0.19
162	0.23	0.20	−0.09	−0.28	−0.20
182	0.19	0.19	−0.03	−0.20	−0.17
205	0.16	0.18	0.01	−0.14	−0.14
233	0.18	0.18	0.05	−0.08	−0.10
267	0.13	0.17	0.10	0.00	−0.08
309	0.11	0.19	0.14	0.05	−0.03
334	0.10	0.19	0.16	0.08	−0.00
362	0.11	0.21	0.19	0.10	0.02
393	0.11	0.22	0.22	0.14	0.06

$$Y(E,T)=\frac{d\sigma/dw}{d\sigma_R/dE}=\frac{d\sigma}{dW}\frac{T}{4\pi a_0^2}\left[\frac{R}{E}\right]^{-2}. \quad (4)$$

Here T is the incident electron energy, E is the electron energy loss, $W+V_{\text{ion}}$, with the ionization potential V_{ion} taken as 14.014 eV,[7] a_0 is the Bohr radius, R is the Rydberg constant taken as 13.6055 eV (Ref. 7), and $d\sigma_R/dE$ is the Rutherford cross section. A plot of $Y(E, T=800$ eV) is given in Fig. 1.

The total ionization cross section σ_{ion} was calculated using the relationship

$$\sigma_{\text{ion}}(T)=4\pi a_0^2\frac{R}{T}\int_{x_1}^{x_2}Y(E,T)d\left[\frac{R}{E}\right], \quad (5)$$

where kinematic limits x_1 and x_2 are $2R/(T+V_{\text{ion}})$ and

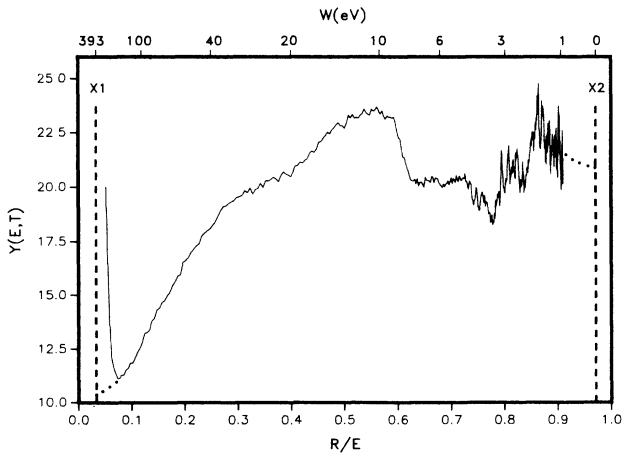

FIG. 1. A Platzman plot $Y(E, T=800$ eV) of e^--CO. Dotted line indicates extrapolation used at low- and high-ejection energies in order to calculate the total ionization cross section.

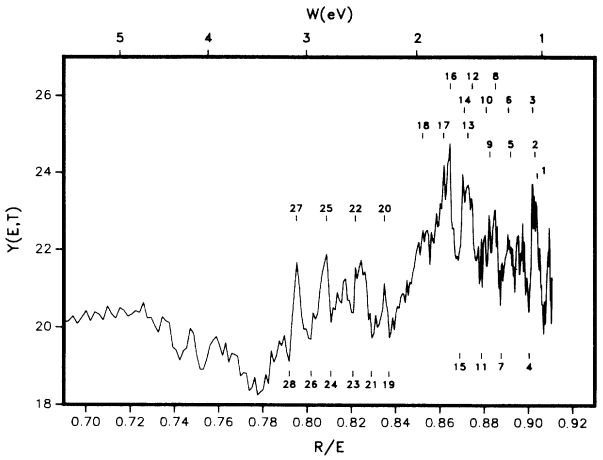

FIG. 2. A Platzman plot $Y(E, T=800$ eV) of e^--CO for the low-ejection energy range. Numbers on the autoionizing lines refer to assignments in Table II.

R/V_{ion}, respectively.

To compute the total ionization cross section σ_{ion}, the Y curve in Fig. 1 was extrapolated on the regions near the x_1 and x_2. The rapid rise near the x_1 limit is due to exchange effects between the scattered and ejected electrons. The extrapolation value of Y at x_1 is between 10 and 11 that represents the effective number of target electrons involved in the ionization process.

From Eq. (5) we obtained the total ionization cross section at $T=800$ eV as 1.10 ± 0.16 (Å)^2. Our result is in excellent agreement with that of Rapp and Englander-Golden [$\sigma_{\text{ion}}(T=800\text{ eV})=1.11$ (Å)^2].[8]

It is obvious from Fig. 1 that there are a large number of autoionization peaks in the lower-ejected energy region ($W<4$ eV). These are believed to be mainly due to the Rydberg series converging to the $A\,^2\Pi$ state and the $B\,^2\Sigma^+$ state decaying to the $X\,^2\Sigma^+$ and $A\,^2\Pi$ ion states. Since both the Rydberg states and the ion states contain a number of vibrational substates, the spectrum is complex, as shown by the expanded low-ejected energy region shown in Fig. 2. From a knowledge of the photoabsorption spectra,[9] we assigned possible autoionization transitions in Table II. Many of these are observed for the first

TABLE II. Some possible autoionization transitions. Corresponding peaks with peak number are shown in Fig. 2. Note: Here $9s\sigma$ belongs to R_B III Rydberg series and the other $ns\sigma$ states belong to R_1 I Rydberg series; $np\pi$ and $nd\pi$ are the states of R_B sharp and IV Rydberg series, respectively.

Peak no.	Energy W (eV)	Possible transitions
1	1.05	$5s\sigma$ ($v'=1$)$\rightarrow X\,^2\Sigma^+$ ($v=3$)
2	1.06	$3d\pi$ ($v'=2$)$\rightarrow A\,^2\Pi$ ($v=4$)
3	1.08	$4s\sigma$ ($v'=2$)$\rightarrow X\,^2\Sigma^+$ ($v=1$)
4	1.10	$4d\pi$ ($v'=1$)$\rightarrow A\,^2\Pi$ ($v=7$)
5	1.24	$3d\pi$ ($v'=2$)$\rightarrow A\,^2\Pi$ ($v=3$)
6	1.26	$4s\sigma$ ($v'=3$)$\rightarrow X\,^2\Sigma^+$ ($v=1$)
7	1.32	$4d\pi$ ($v'=1$)$\rightarrow A\,^2\Pi$ ($v=6$)
8	1.36	$4s\sigma$ ($v'=2$)$\rightarrow X\,^2\Sigma^+$ ($v=0$)
9	1.41	$3d\pi$ ($v'=2$)$\rightarrow A\,^2\Pi$ ($v=2$)
10	1.44	$4s\sigma$ ($v'=4$)$\rightarrow X\,^2\Sigma^+$ ($v=1$)
11	1.46	$4d\pi$ ($v'=1$)$\rightarrow A\,^2\Pi$ ($v=5$)
12	1.55	$4s\sigma$ ($v'=3$)$\rightarrow X\,^2\Sigma^+$ ($v=0$)
13	1.58	$5s\sigma$ ($v'=1$)$\rightarrow X\,^2\Sigma^+$ ($v=1$)
14	1.62	$4s\sigma$ ($v'=5$)$\rightarrow X\,^2\Sigma^+$ ($v=1$)
15	1.66	$4d\pi$ ($v'=1$)$\rightarrow A\,^2\Pi$ ($v=4$)
16	1.73	$4s\sigma$ ($v'=4$)$\rightarrow X\,^2\Sigma^+$ ($v=0$)
17	1.78	$5s\sigma$ ($v'=2$)$\rightarrow X\,^2\Sigma^+$ ($v=1$)
18	1.95	$5s\sigma$ ($v'=3$)$\rightarrow X\,^2\Sigma^+$ ($v=1$)
19	2.20	$9s\sigma$ ($v'=1$)$\rightarrow A\,^2\Pi$ ($v=5$)
20	2.28	$3p\pi$ ($v'=0$)$\rightarrow X\,^2\Sigma^+$ ($v=3$)
21	2.39	$9s\sigma$ ($v'=1$)$\rightarrow A\,^2\Pi$ ($v=4$)
22	2.54	$3p\pi$ ($v'=0$)$\rightarrow X\,^2\Sigma^+$ ($v=2$)
23	2.56	$9s\sigma$ ($v'=1$)$\rightarrow A\,^2\Pi$ ($v=3$)
24	2.73	$9s\sigma$ ($v'=1$)$\rightarrow A\,^2\Pi$ ($v=2$)
25	2.81	$3p\pi$ ($v'=0$)$\rightarrow X\,^2\Sigma^+$ ($v=1$)
26	2.92	$9s\sigma$ ($v'=1$)$\rightarrow A\,^2\Pi$ ($v=1$)
27	3.09	$3p\pi$ ($v'=0$)$\rightarrow X\,^2\Sigma^+$ ($v=0$)
28	3.12	$9s\sigma$ ($v'=1$)$\rightarrow A\,^2\Pi$ ($v=0$)

All experimental data[10] have been deposited with the Physics Auxiliary Publication Service (PAPS).

The authors would like to acknowledge support by National Science Foundation Grant No. CHE86-00746.

[1]C. B. Opal, E. C. Beaty, and W. K. Peterson, At. Data **4**, 209 (1972).

[2]R. R. Goruganthu and R. A. Bonham, Phys. Rev. A **34**, 103 (1986); R. R. Goruganthu, W. G. Wilson, and R. A. Bonham, *ibid.* **35**, 540 (1987).

[3]R. D. DuBois and M. E. Rudd, J. Phys. B **9**, 2657 (1976).

[4]Ch. K. Kwan, Y.-F. Hsieh, W. E. Kauppila, S. J. Smith, T. S. Stein, and M. N. Uddin, Phys. Rev. A **27**, 1328 (1983).

[5]R. R. Goruganthu and W. G. Wilson, Rev. Sci. Instrum. **55**, 2030 (1984).

[6]Y. K. Kim, Radiat. Res. **61**, 21 (1975); **64**, 96 (1975); **64**, 205 (1975).

[7]J.-H. Fock, P. Gurtler, and E. E. Koch, Chem. Phys. **47**, 87 (1980).

[8]D. Rapp and P. Englander-Golden, J. Chem. Phys. **43**, 1464 (1965).

[9]M. Ogawa and S. Ogawa, J. Mol. Spectrosc. **41**, 393 (1972).

[10]See AIP document No. PAPS PLRAA-38-2160-03 for 3 pages of the original experimental data. Order by PAPS number and journal reference from American Institute of Physics, Physics Auxiliary Publication Service, 335 East 45th Street, New York, N.Y. 10017. The prepaid price is $1.50 for each microfiche or $5.00 for a photocopy. Airmail additional.